Structures, Electronic States, and Electroluminescent Properties of a Zinc(II) 2-(2-Hydroxyphenyl)benzothiazolate Complex

Gui Yu, Shiwei Yin, Yunqi Liu,* Zhigang Shuai, and Daoben Zhu*

Contribution from the Center for Molecular Science, Institute of Chemistry, Chinese Academy of Sciences, Beijing 100080, P. R. China

Received July 9, 2003; E-mail: liuyq@iccas.ac.cn

Abstract: Bis(2-(2-hydroxyphenyl)benzothiazolate)zinc ($Zn(BTZ)_2$) is one of the best white electroluminescent materials used in organic light-emitting diodes (LEDs). Despite a large number of studies devoted to this complex, very little is known about its basic molecular and electronic structures and electron transport properties in LEDs. Therefore, we investigate the structures and electroluminescent properties. The unsolvated single crystal of $Zn(BTZ)_2$ was grown and its crystalline structure was determined from X-ray diffraction data. The crystal is triclinic, space group P-1, $a = 9.4890(19)$ Å, $b = 9.5687(19)$ Å, $c = 11.685(2)$ Å, $\alpha = 84.38(3)°$, $\beta = 78.94(3)°$, $\gamma = 83.32(3)°$. The structure of the chelate is dimeric $[Zn(BTZ)_2]_2$ with two isotropic Zn^{2+} ion centers having five-coordinate geometry. The present study provides direct evidence for the sole existence of dimeric structure in the powder and the thin film. The dimer is energetically more stable than the monomer. Analysis of the electronic structure of $[Zn(BTZ)_2]_2$ calculated by density functional theory reveals a localization of orbital and the distribution of four orbital "tetrads". The structural stabilities of both anion and cation and the distribution of the hole in the cation and that of the excess electron in the anion are discussed in terms of theoretical calculations. Strong intermolecular interaction may be expected to enable good electron transport properties as compared with tris(8-hydroxyquinolinato)aluminum.

Introduction

Since the reports by C. W. Tang[1] and J. H. Burroughes,[2] organic and polymer light-emitting diodes (LEDs) have received considerable attention due to their potential application in various displays.[3-8] The organic and polymer devices offer the clear advantages over inorganic counterparts, such as low cost and high luminous efficiency. These devices are able to produce all emission colors in accordance with a wide selection of organic emitting materials. Emitting materials for organic LEDs can be classified into three types according to their molecular structures: organic dyes,[9] chelate metal complexes,[1] and polymers.[2] Motivated by the success of tris(8-hydroxyquinolinato)aluminum (Alq_3) in vacuum-deposited LEDs, organic chelate metal complexes have in particular attracted a lot of attentions.[10-12] Organic metal complexes offer many attractive properties such as displaying a double role of electron transport and light emission, higher environmental stability, ease of sublimation, and a much greater diversity of tunable electronic properties by virtue of the coordinated metal center. The major drawback of the metal complexes, however, is their low electron transport ability. A typical cell structure for multilayer organic LEDs is the following: an anode (indium tin oxide (ITO) on a glass substrate)/a hole transport layer/a light emitting layer/an electron transport layer/a cathode.[1] Electrons from the cathode and holes from the anode travel through the transport layer until they form an exciton that decays, giving rise to electroluminescence. Therefore, balance of carrier injection and transport are necessary to obtain highly effective LEDs. Alq_3 is one of the best known electron transport materials with high mobility. However, the mobility of Alq_3 is lower than that of hole

* Corresponding authors.
(1) Tang, C. W.; Vanslyke, S. A. *Appl. Phys. Lett.* **1987**, *51*, 913.
(2) Burroughes, J. H.; Bradly, D. D. C.; Broun, A. R.; Marks, R. N.; Mackay, K.; Friend, R. H.; Burn, P. L.; Holmes, A. B. *Nature* **1990**, *347*, 539.
(3) Gustafsson, G.; Cao, Y.; Treacy, G. M.; Klavetter, F.; Colaneri, N.; Heeger, A. J. *Nature* **1992**, *357*, 477.
(4) (a) Baldo, M. A.; O'Brien, D. F.; You, Y.; Shoustikov, A.; Sibley, S.; Thompson, M. E.; Forrest, S. R. *Nature* **1998**, *395*, 151. (b) Baldo, M. A.; Lamansky, S.; Burrows, P. E.; Thompson, M. E.; Forrest, S. R. *Appl. Phys. Lett.* **1999**, *75*, 4. (c) Baldo, M. A.; Thompson, M. E.; Forrest, S. R. *Nature* **2000**, *403*, 750. (d) Tamayo, A. B.; Alleyne, B. D.; Djurovich, P. I.; Lamansky, S.; Tsyba, I.; Ho, N. N.; Bau, R.; Thompson, M. E. *J. Am. Chem. Soc.* **2003**, *125*, 7377. (e) Sudhakar, M.; Djurovich, P. I.; Hogen-Esch, T. E.; Thompson, M. E. *J. Am. Chem. Soc.* **2003**, *125*, 7796.
(5) (a) Handy, E. S.; Pal, A. J.; Rubner, M. F.; *J. Am. Chem. Soc.* **1999**, *121*, 3525. (b) Gao, F. G.; Bard, A. J. *J. Am. Chem. Soc.* **2000**, *122*, 7426. (c) Buda, M.; Kalyuzhny, G.; Bard, A. J. *J. Am. Chem. Soc.* **2002**, *124*, 6090.
(6) (a) Chen, F. C.; Yang, Y. *Appl. Phys. Lett.* **2002**, *80*, 2308. (b) He, G. F.; Chang, S. C.; Chen, F. C.; Li, Y. F.; Yang, Y. *Appl. Phys. Lett.* **2002**, *81*, 1509.
(7) Welter, S.; Brunner, K.; Hofstraat. J. W.; Cola, L. D. *Nature* **2003**, *421*, 54.
(8) (a) Yu, G.; Liu, Y. Q.; Wu, X.; Zheng, M.; Bai, F. L.; Zhu, D. B.; Jin, L. P.; Wang, M. Z.; Wu, X. N. *Appl. Phys. Lett.* **1999**, *74*, 2295. (b) Yu, G.; Liu, Y. Q.; Wu, X.; Zhu, D. B.; Li, H. Y.; Jin, L. P.; Wang, M. Z. *Chem. Mater.* **2000**, *12*, 2537. (c) Yu, G.; Liu, Y. Q.; Zhou, S. Q.; Bai, F. L.; Zeng, P. J.; Wu, X.; Zheng, M.; Zhu, D. B. *Phys. Rev. B* **2002**, *65*, 115211.
(9) Adachi, C.; Tsutsui, T.; Saito, S. *Appl. Phys. Lett.* **1990**, *56*, 799.
(10) Hopkins, T. A.; Meerholz, K.; Shaheen, S.; Anderson, M. L.; Schmidt, A.; Kippelen, B.; Padias, A. B.; Hall, Jr. K. K.; Peyghambarian, N.; Armstrong, N. R.; *Chem. Mater.* **1996**, *8*, 344.
(11) Sapochak, L. S.; Padmaperuma, A.; Washton, N.; Endrino, F.; Schmett, G. T.; Marshall, J.; Fogarty, D.; Burrows, P. E.; Forrenst, S. R. *J. Am. Chem. Soc.* **2001**, *123*, 6300.
(12) Wang, J. F.; Wang, R. Y.; Yang, J.; Zheng, Z. P.; Carduct, M. D.; Cayou, T.; Peyghambarian, N.; Jabbour, G. E. *J. Am. Chem. Soc.* **2001**, *123*, 6179.

transport materials, such as *N*,*N*′-diphenyl-*N*,*N*′-bis(1-naphenyl)-1,1′-biphenyl-4,4′-diamine (NPB) and *N*,*N*′-diphenyl-*N*,*N*′-di-(3-methylphenyl)-1,1′-biphenyl-4,4′-diamine (TPD). In an organic LED using NPB or TPD as the hole transport layer and Alq$_3$ as the electron transport layer, the hole and electron transports will be unbalanced. Due to this fact, it is desirable to design molecules with high electron mobility.

The photoluminescence (PL) quantum efficiency, volatility, film-forming properties, charge transport properties, energy band offsets of organic layers, and environmental stability are key factors for determining electroluminescence (EL) properties of organic materials. These parameters are strongly coupled to molecular structure and bulk molecular packing characteristics.[13] However, there are few investigations of the correlations existing between the molecular packing, the morphological properties in thin films, and the corresponding optical/electronic properties in organic/polymeric materials.[14] Alq$_3$ has two geometric isomers, the meridianal (*mer*-Alq$_3$) and facial (*fac*-Alq$_3$) forms having C_1 and C_3 symmetric, respectively. The two isomers of Alq$_3$ give rise to different stability, distinct electronic behavior, and inhomogeneously broadened spectra.[15,16] Simultaneously, in the case of *mer*-Alq$_3$, the solvated and unsolvated molecular structures are different, which leads to a large variety of optical behaviors.[14] Therefore, it is important to obtain the single crystal because X-ray diffraction on single crystals is the best method for providing their molecular structure and packing.

With the assistance of quantum chemical calculations, the ground- and excited-state properties and the effect of charge addition on the electronic structure and the molecular geometry for both the *mer*-Alq$_3$ and the *fac*-Alq$_3$ have been reported as well as the bonding characteristics in metal-Alq$_3$.[16−21] It has been found that the meridianal isomer is more thermodynamically stable, but under certain chemical conditions, the facial isomer can become the preferred form. Density functional theory (DFT) calculation has been recently carried out to investigate the electronic properties of cyclometalated Ir and Pt compounds.[22−24] Nevertheless, few theoretical calculations of other kinds of chelates have so far been reported.

Bis(2-(2-hydroxyphenyl)benzothiazolate)zinc (Zn(BTZ)$_2$) has been studied as an excellent white EL material.[25,26] However, the molecular structure, electronic characteristics, and electron transport properties of the complex have not yet been reported to the best of our knowledge. In this paper, we present a theoretical and experimental investigation of the molecular and electronic structures of 2-(2-hydroxyphenyl)benzothiazolate

chelate of zinc(II) and its performances in organic LEDs. Single-crystal X-ray diffraction of the chelate shows that the molecular structure of the material is dimer [Zn(BTZ)$_2$]$_2$. Theoretical calculations of the total energies of Zn(BTZ)$_2$ and [Zn(BTZ)$_2$]$_2$ molecules reveal that the dimer is energetically more stable than the monomer. The existence of the dimeric structure in powder and amorphous vacuum-deposited thin film is supported by differential scanning calorimetry (DSC) and spectroscopic methods.

Calculation of the location and distribution of the orbitals in the [Zn(BTZ)$_2$]$_2$ molecule shows that the highest occupied molecular orbitals (HOMO's) are mainly localized on two nonbridging ligands, and the lowest unoccupied molecular orbitals (LUMO's) are localized predominantly on two bridging ligands. Analysis of the structural and electronic properties for both the anion and the cation reveals a relatively highly structural stability versus injection of one charge, whether positive or negative. Treatment of the molecular packing shows that the ligands are involved in strong $\pi-\pi$ stacking, which may be expected to result in enhanced electron transport in organic LEDs. We compare the electron transport of the zinc complex with the well-known emitter Alq$_3$ in organic LEDs under the same experimental conditions by taking advantage of the combinatorial approach.

Experimental Section

Material Synthesis and Structural Characterization. Zn(BTZ)$_2$ was synthesized from the complex reaction between zinc acetate dihydrate and 2-(2-hydroxyphenyl)benzothiazolate.[26] The final powder was purified by the train sublimation method. Anal. Calcd for C$_{26}$H$_{16}$N$_2$O$_2$S$_2$Zn (%): C, 60.47; H, 3.13; N, 5.43. Found: C, 60.44; H, 2.99; N, 5.34. FT IR (KBr) (cm^{-1}) 3061, 2924, 1604, 1542, 1487, 1422, 1347,1321, 1208, 1158, 1132, 1037. Elemental analyses were performed on a Perkin-Elmer 240C elemental analyzer for C, H, and N determinations. FT-IR spectrum of the complex dispersed in KBr disks was recorded on a Bio-Rad TFs156 spectrometer.

Single-Crystal Growth. A single crystal of [Zn(BTZ)$_2$]$_2$ was obtained by vacuum sublimation in a tube furnace under a base pressure of <10^{-4} Pa at 240 °C for 48 h. The single crystal collected at 210 °C has a typical size of 0.64 × 0.57 × 0.29 mm. The annealing experiment was performed with Perkin-Elmer thermogravimeter (model TGA7). A sample of the single crystal was heated under a nitrogen atmosphere at 280 °C for about 2 h.

X-ray Diffraction. Crystal data were obtained with graphine-monochromated Cu Kα radiation ($\lambda = 0.710\,73$ Å) on a Rigaku RAPID IP imaging plate system. The structure was solved by direct method with SHELXL97 program and refined with full-matrix least-squares methods.

Thermal Analysis. Thermogravimetric analysis (TGA) was carried out using a Perkin-Elmer thermogravimeter (model TGA7) under a dry nitrogen gas flow at a heating rate of 20 °C/min. Glass transition temperature (T_g) and melting point (T_m) of the complex were determined by differential scanning calorimeter (DSC) using a Perkin-Elmer differential scanning calorimeter (DSC7).

Computational Method. The quantum chemical calculations for Zn(BTZ)$_2$ and its dimer were carried out with LDA-DFT as implemented in the DMol3 package.[27,28] The basis set chosen is the double numerical plus d-function (DND). The local functional for the exchange-correlation potential is the Perden-Wang LDA functional (PWC).[29] The core electrons for metals were treated by effective core potentials (ECP).

(13) Sapochak, S. L.; Burrows, P. E.; Garbuzov, D.; Ho, D. M.; Forrest, S. R.; Thompson, M. E. *J. Phys. Chem.* **1996**, *100*, 17766.
(14) Brinkmann, M.; Gadret, G.; Muccini, M.; Taliani, C.; Masciocchi, N.; Sironi, A. *J. Am. Chem. Soc.* **2000**, *122*, 5147.
(15) Sano, K.; Kawata, Y.; Urano, T. I.; Mori, Y. *J. Mater. Chem.* **1992**, *2*, 767.
(16) Curioni, A.; Boero, M.; Andreoni, W. *Chem. Phys. Lett.* **1998**, *294*, 263.
(17) Halls, M. D.; Schlegel, H. B. *Chem. Mater.* **2001**, *13*, 2632.
(18) Curioni, A.; Andreoni, W. *J. Am. Chem. Soc.* **1999**, *121*, 8216.
(19) Curioni, A.; Andreoni, W. *Appl. Phys. Lett.* **1998**, *72*, 1575.
(20) Kushto, G. P.; Iizumi, Y.; Kido, J.; Kafafi, Z. H. *J. Phys. Chem. A* **2000**, *104*, 3670.
(21) Halls, M. D.; Aroca, R. *Can. J. Chem.* **1998**, *76*, 1730.
(22) Hay, P. J. *J. Phys. Chem. A* **2002**, *106*, 1634.
(23) Brooks, J.; Babayan, Y.; Lamansky, S.; Djurovich, P. I.; Tsyba, I.; Bau, R.; Thompson, M. E. *Inorg. Chem.* **2002**, *41*, 3055.
(24) Tamayo, A. B.; Alleyne, B. D.; Djurovich, Lamansky, S.; P. I.; Tsyba, I.; HO, N. N.; Bau, R.; Thompson, M. E. *J. Am. Chem. Soc.* **2003**, *125*, 7377.
(25) Sano, T.; Nishio, Y.; Hamada, Y. J.; Takahashi, H.; Usiki, T.; Shibata, K. *J. Mater. Chem.* **2000**, *10*, 157.
(26) Hamada, Y.; Sano, T.; Fujii, H.; Nishio, Y.; Takahashi, H.; Shibata, K. *Jpn. J. Appl. Phys.* **1996**, *35*, L1339.

(27) Delley, B. *J. Chem. Phys.* **1990**, *92*, 508.
(28) Delley, B. *J. Chem. Phys.* **2000**, *113*, 7756.
(29) Perdew, J. P.; Wang, Y. *Phys. Rev. B* **1992**, *45*, 13244.

Table 1. Experimental and Calculated Structural Parameters for the [Zn(BTZ)$_2$]$_2$ Molecule

structural parameter[a]	exptl	exptl[b]	calcd	structural parameter[a]	exptl	exptl[b]	calcd
Zn(1)−O(1)	1.962	1.958	1.968	O(1)−Zn(1)−N(1)	87.37	87.24	89.34
Zn(1)−O(2A)	2.017	2.017	1.963	O(2A)−Zn(1)−N(1)	120.09	119.72	120.70
Zn(1)−O(2)	2.058	2.060	2.107	O(2)−Zn(1)−N(1)	99.63	100.06	93.00
Zn(1)−N(1)	2.095	2.103	2.024	O(1)−Zn(1)−N(2)	97.26	96.96	97.05
Zn(1)−N(2)	2.170	2.178	2.054	O(2A)−Zn(1)−N(2)	117.12	117.63	125.32
O(1)−Zn(1)−O(2A)	97.40	97.54	102.87	O(2)−Zn(1)−N(2)	82.13	82.05	82.94
O(1)−Zn(1)−O(2)	172.18	172.03	177.50	N(1)−Zn(1)−N(2)	121.38	121.30	109.77
O(2A)−Zn(1)−O(2)	76.13	76.11	75.20	Zn(1A)−O(2)−Zn(1)	103.87	103.89	104.80

[a] Bond lengths are reported in angstroms and bond angles in degrees. [b] The single crystal is annealed under a nitrogen atmosphere at 280 °C for about 2 h.

Device Preparation. NPB and Alq$_3$ (purchased from Aldrich Chemical Co.) were purified by a train sublimation method. The organic EL devices were fabricated on a glass substrate coated with ITO (sheet resistance 30 Ω/□) using a conventional vacuum vapor deposition in a vacuum of 2×10^{-4} Pa. The emitting area of the EL devices was 4 mm^2. The organic layers were grown by means of conventional vacuum deposition. Finally, aluminum was evaporated as a cathode. A quartz crystal oscillator placed near the substrate was used to measure the thickness of the thin films, which were calibrated ex situ using an Ambios Technology XP-2 surface profilometer. The absorption spectra of Zn(BTZ)$_2$ thin films were studied using the quartz substrates.
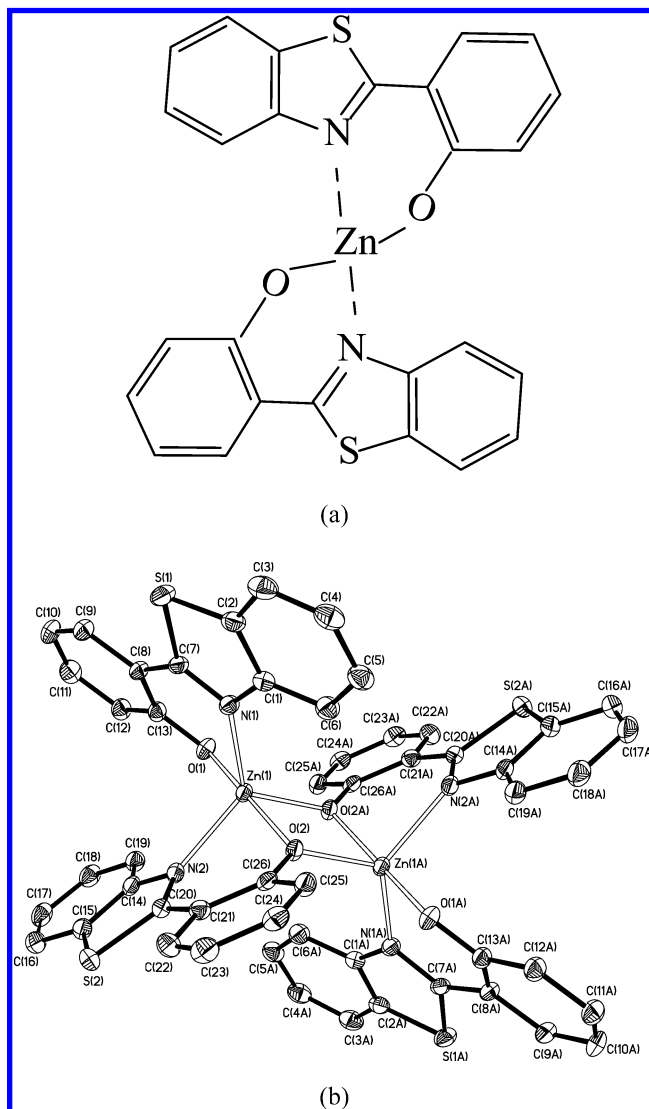
The absorption spectra were recorded with a General TU-1201 UV−vis spectrophotometer. Brightness, chromaticity coordinates, and EL spectra were measured with a SpectraScan PR 650 photometer. Current−voltage (I−V) characteristics were measured with a Hewlett-Packard 4140B semiconductor parameter analyzer. All the measurements were performed under ambient atmosphere at room temperature.

Results and Discussion

Molecular Structure and X-ray Single-Crystal Diffraction. Most of metal complexes may exist as a monomer in their crystals. In contrast, anhydrous 8-hydroxyquinolinato zinc crystals have a tetrameric structure (Znq$_2$)$_4$ with two distinct Zn^{2+} ion centers with six- and five-coordinate geometry, respectively.[30,31] To describe the molecular structure of 2-(2-hydroxyphenyl)benzothiazolate zinc, the single crystal was grown. The chemical and crystal structures of the zinc complex are shown in Figure 1. The bond lengths and bond angles are listed in Table 1. As seen in Figure 1, the zinc complex exists as an anhydrous dimer. The zinc ions are five-coordinate to the benzothiazole ligands and have distorted trigonal bipyramidal geometry. Two of the 2-(2-hydroxyphenyl)benzothiazole ligands are involved in the Zn atoms only. The Zn−O bond lengths for the nonbridging ligands are 1.962 Å, whereas those in the two bridging ligands lengthen to 2.058 Å. Similar behavior is observed for the Zn−N bond lengths.

The formation of the bridges leads to a weaker interaction between the bridging ligands and the zinc ions and to longer bonds in two bridging ligands. The Zn−O and Zn−N bond lengths are similar to those observed in the tetramer (Znq$_2$)$_4$.[31] In the triclinic crystal structure [Zn(BTZ)$_2$]$_2$ molecules are arranged so that one inversion center is located at the dimer center and the parallel veins center through the phenoxido oxygens. The former results in an inversion symmetry for the [Zn(BTZ)$_2$]$_2$ molecule (point group-1); the latter forces parallel arrangement of the parallel veins and terminal ligands on the

(30) Kai, Y.; Morita, M.; Yasuoka, N.; Kasai, N. *Bull. Chem. Soc. Jpn.* **1985**, *58*, 1631.
(31) Sapochak, L. S.; Benincasa, F. E.; Schofield, R. S.; Baker, J. L.; Riccio, K. K. C.; Fogarty, D.; Kohlmann, H.; Ferris, K. F.; Burrows, P. E. *J. Am. Chem. Soc.* **2002**, *124*, 6119.
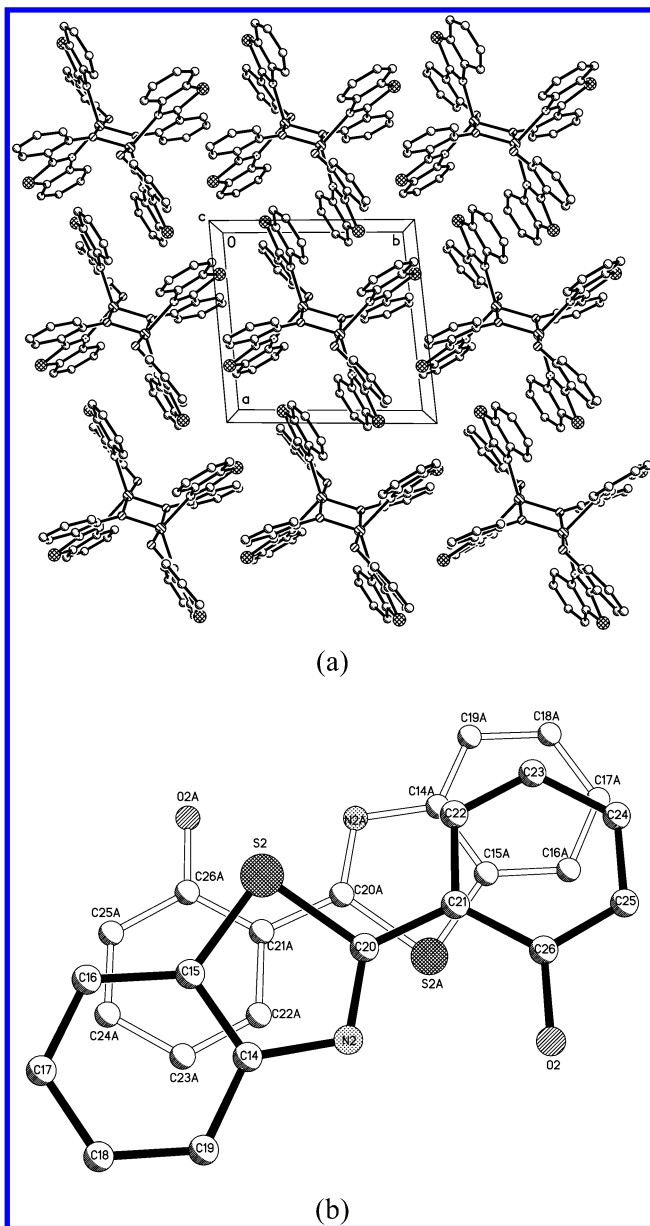
Figure 1. Chemical (a) and molecular (b) structures of the Zn complex.

adjacent dimeric units and results in a close intermolecular π−π interaction of 3.7653 Å (see Figure 2a). The π−π stacking occurs in the phenoxido and the benzothiazolyl moieties of adjacent 2-(2-hydroxyphenyl)benzothiazole ligands as shown in Figure 2b. This intermolecular interaction will lead to good carrier transport properties.

Dimer Structural and Thermal Stabilities. To validate the morphological and molecular stabilities of the dimeric structure in the single crystal, a sample of the single crystal [Zn(BTZ)$_2$]$_2$ was heated under a nitrogen atmosphere at 280 °C for about 2 h. Annealing temperatures higher than 300 °C are found to result

Figure 2. Crystal packing of the $[Zn(BTZ)_2]_2$ (a) and intermolecular interaction of the bridging ligands (b).

Table 2. Summary of Crystal Data for Nonannealing and Annealing $[Zn(BTZ)_2]_2$, Including Data Collection and Refinement Details

	nonannealing	annealing
empirical formula	$C_{26}H_{16}N_2O_2S_2Zn$	$C_{26}H_{16}N_2O_2S_2Zn$
fw	517.90	517.90
cryst syst	triclinic	triclinic
space group	*P*-1	*P*-1
a, Å	9.4890(19)	9.5159(5)
b, Å	9.5687(19)	9.5888(6)
c, Å	11.685(2)	11.7126(9)
α, deg	84.38(3)	84.2290(18)
β, deg	78.94(3)	79.011(5)
γ, deg	83.32(3)	83.5380(11)
V, Å^3	1031.1(4)	1039.03(12)
Z	2	2
$F(000)$	528	528
D(calcd), mg m^{-3}	1.668	1.655
μ, mm^{-1}	1.423	1.412
temp, K	293(2)	293(2)
λ, Å	0.710 73	0.710 73
2θ range, deg	2.15−27.44	2.14−27.48
final R indices [$I > 2\sigma(I)$]	$R1 = 0.0566$	$R1 = 0.0296$
	$wR2 = 0.1452$	$wR2 = 0.0698$
R indices (all data)	$R1 = 0.0635$	$R1 = 0.0421$
	$wR2 = 0.1491$	$wR2 = 0.0722$
goodness-of-fit on $F\wedge2$	1.072	0.944

Table 3. Calculated Total Energies and Dipole Moments for the $[Zn(BTZ)_2]_n$ Series

$[Zn(BTZ)_2]_n$	total energy, au	dipole moment, D
$Zn(BTZ)_2$, monomer	−2270.433 889 0	4.3481
$[Zn(BTZ)_2]_2$, dimer	−4540.915 470 7	0

of the monomers of the optimized dimer structure was removed to form a monomer. The calculated total energy and dipole moments for both the $Zn(BTZ)_2$ and $[Zn(BTZ)_2]_2$ molecules are given in Table 3. In our calculations of the zinc complexes, $[Zn(BTZ)_2]_2$ turns out to be lower in energy as compared to two $Zn(BTZ)_2$ by 39.7 kcal/mol. While this energy does not include thermal and entropic effects, the overall magnitudes are reasonable to expect that the dimer is thermodynamically favored over the monomer. A similar result has been observed for the $(Znq_2)_n$ oligomers ($n = 1, 2, 4$).[31] Their theoretical calculation showed that the dimer was a lower energy configuration as compared to the two monomers and the tetramer was energetically preferred over the two dimers. Note that $Zn(BTZ)_2$ and $[Zn(BTZ)_2]_2$ have different dipole moments, which explain their different melting points.

To evidence the unique presence of the dimer in powder, we report the results obtained from thermal analysis characterization. The zinc complex is reasonably stable upon exposure to air and exhibited high thermal stability. The TGA and DSC scans for $[Zn(BTZ)_2]_2$ powder are shown in Figures 3 and 4. We observe a single endothermic transition at 310 °C with only a 1% weight loss prior to decomposition of the material at 415 °C. However, the morphological stability of Alq$_3$ has been attributed to its intrinsic polymorphic nature. Several phase transitions were observed for Alq$_3$ in addition to a large melting transition (T_m) at 419 °C, and the additional exothermic transition at 396 °C was attributed to a phase transition from the α-Alq$_3$ to the γ-Alq$_3$ phase.[11] If other oligomeric species were present or formed by molecular rearrangement during fusion of $[Zn(BTZ)_2]_2$, an additional enthalpic transition would be expected to become resolved at slower heating rates. Figure
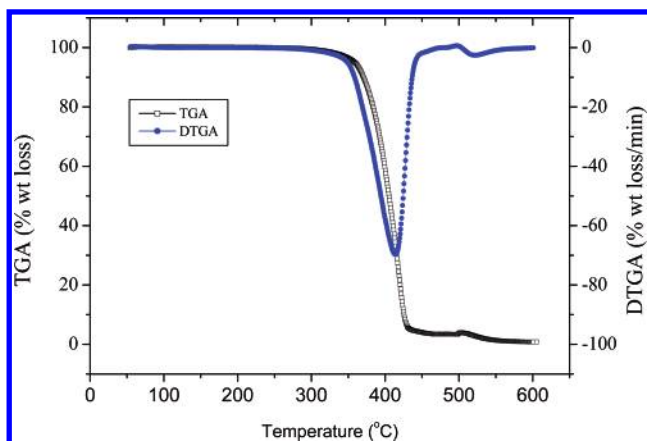
in fusion of the sample. For comparison, we also report the structural parameters obtained from annealing $[Zn(BTZ)_2]_2$. The annealing single crystal exhibits the same summary of crystal data, bond lengths, and bond angles (see Tables 1 and 2). Phase transitions were not observed for the annealing sample. These results indicate that the single crystal has good morphological, structural, and molecular stabilities.

A number of theoretical studies of the electronic structure of Alq$_3$ and $(Znq_2)_2$ have been reported, which complement the extensive experimental investigations.[14,28] Interpretation of the observed spectral features is greatly assisted by molecular orbital calculations. To better provide the electronic structure of $[Zn(BTZ)_2]_2$, the geometric parameters employed in the quantum chemical calculation are from the crystal structure data, which are quite close to the DFT optimized structure (see Table 1). For the sake of comparison, molecular orbital calculations were also carried out for the monomer $Zn(BTZ)_2$. Because crystallographic coordinates are not available for the monomer, one
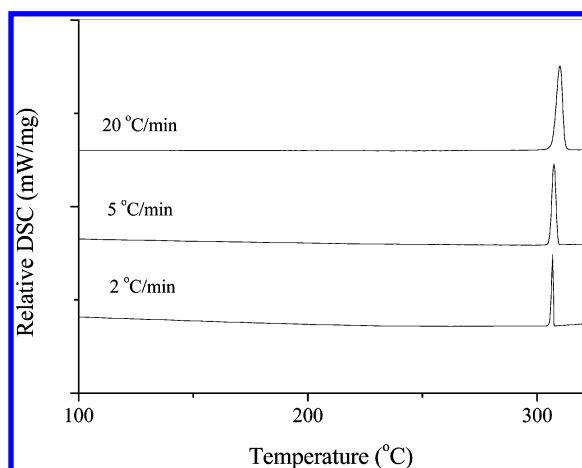
Figure 3. TGA and DTGA curves of the [Zn(BTZ)$_2$]$_2$ powder.

Figure 4. DSC curves of the [Zn(BTZ)$_2$]$_2$ powder at different heating rates.

4 shows the DSC scans for powder [Zn(BTZ)$_2$]$_2$ observed at different heating rates. A single endothermic transition (ΔH_{fusion} = 113.68 J/mol) is obtained, which narrows with a decreasing heating rate. Similar behavior was observed for (Znq$_2$)$_4$; thus, it is reasonable to expect that the dimer in the powder exists uniquely.[31] The single crystal [Zn(BTZ)$_2$]$_2$ was obtained by high-vacuum temperature sublimation of the powder sample, which was purified by the train sublimation method. Analysis of the single crystal and powder samples by ^{1}H NMR spectroscopy in CDCl$_3$ showed identical results. Moreover, we found no detectable changes in the FT-IR spectra comparing vapor-deposited thin films, the single crystal, and powder sample dispersed in KBr. These results support the uniqueness of the dimer in the single crystal, in the powder purified by the train sublimation method, and in the vacuum-deposited thin film.

Electronic Structure. In Figure 5, we show the HOMO's and LUMO's of the Zn chelate [Zn(BTZ)$_2$]$_n$ oligomers ($n = 1$, 2). The filled π orbitals (or HOMO's) and the unfilled orbitals (or LUMO's) are mainly dominated by orbitals originating from the 2-(2-hydroxyphenyl)benzothiazolate ligands in all cases. The contribution of Zn^{2+} ions of all these orbitals are vanishingly small. Previous works for Alq$_3$ and (Znq$_2$)$_n$ oligomers have shown that the electron density of the HOMO is localized mainly on the phenoxido ring, and inversely the LUMO is localized on the heterocyclic ring. A similar result is observed for the HOMO's of [Zn(BTZ)$_2$]$_2$, which is localized on the phenoxido ring of the two nonbridging ligands, whereas their LUMO distributes on the phenoxido and thiazolyl rings of the two

bridging ligands. Therefore, the electronic $\pi-\pi^*$ transition in [Zn(BTZ)$_2$]$_2$ is localized on the benzothiazolate ligands, from the nonbridging ligands to the bridging ligands. The phenoxido π system in [Zn(BTZ)$_2$]$_2$ is the highest energy filled state, and hence oxidizing agents will attack the molecule at the phenoxido side of the ligands, making it the most likely site of the trapped hole. In contrast, the thiazolyl system is the lowest-energy vacant state, making it the site of reduction, and thus the trapped electron.
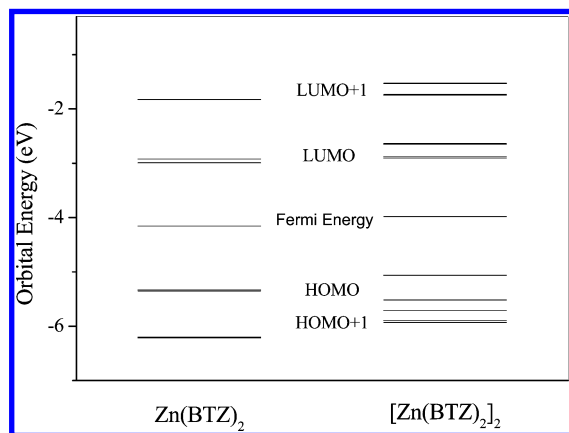
A diagram of the calculated orbital energy level for Zn(BTZ)$_2$ and [Zn(BTZ)$_2$]$_2$ molecules is illustrated in Figure 6. We compare the electronic structure of two (Znq$_2$)$_n$ oligomers and observe that the molecular orbitals of [Zn(BTZ)$_2$]$_2$ are more strongly localized than that in Zn(BTZ)$_2$. The four HOMO's of the [Zn(BTZ)$_2$]$_2$ molecule split in energy and the two highest bound orbitals in the HOMO's tetrad are mainly localized on the two nonbridging ligands, whereas the other orbitals are predominantly on the bridging ligands. Moreover, the LUMOs split in a similar way, but the sequence is reversed: the two lowest-lying states in each "tetrad" are localized predominantly on the two bridging ligands, while the higher states on the two nonbridging ligands.

Ultraviolet Photoelectron Spectroscopy (UPS). The operating voltages and efficiency of EL devices can be dependent on the barriers to charge into the luminescent layer, in addition to internal resistance effects. The charge injection barriers are due mainly to energetic differences between the work function of the electrodes and energy of the HOMO's or LUMO's for organic material. Usually, UPS is one of the simplest and practical methods to give much information needed to reveal the electronic structures of materials. Ionization potential (IP) and the energy level of the HOMO's can be measured by UPS. The UPS spectrum was recorded with a sample bias of -4.0 V to allow observation of the inelastic electron cutoff. A clean Au film on a Si substrate was used for the Fermi level (E_F) and the binding energy calibrations. Its inelastic electron cutoff and its highest occupied states (HOS's) of the HOMO's are enlarged as well. According to the values of the cutoff and the HOS, IP could be obtained as IP = 21.2 − (25.25 − 9.46) eV = 5.41 eV. The [Zn(BTZ)$_2$]$_2$ thin film has a broad absorption with two maxima at 301 and 412 nm, which are caused by the $\pi-\pi^*$ transition of the ligand. By extrapolating the absorption spectrum at the long wavelength side, the optical band gap is evaluated to be about 2.76 eV. Therefore, the LUMO's energy level location is determined to be − 2.65 eV below the vacuum level.

Cation and Anion Properties. To reveal the effects of charge injection on the molecular conformational stability, we calculated structural and electronic properties of both the anion and the cation. For this purpose, geometry optimization was carried out on both molecular ions (i.e., the neutral [Zn(BTZ)$_2$]$_2$ molecule in the presence of an extra electron and that of an extra hole, respectively). The optimized structures for both the cation and the anion show small structural changes relative to the neutral [Zn(BTZ)$_2$]$_2$ molecule. The distribution of the extra hole in the cation calculated as excess spin densities (Figure 7a) is completely localized on the phenoxido rings of both nonbridging ligands and is spatially similar to the HOMO's of the neutral molecule. A different result is found in the anion, where the distribution of the electron as shown in Figure 7b is mainly localized on the phenoxido and thiazolyl rings of both
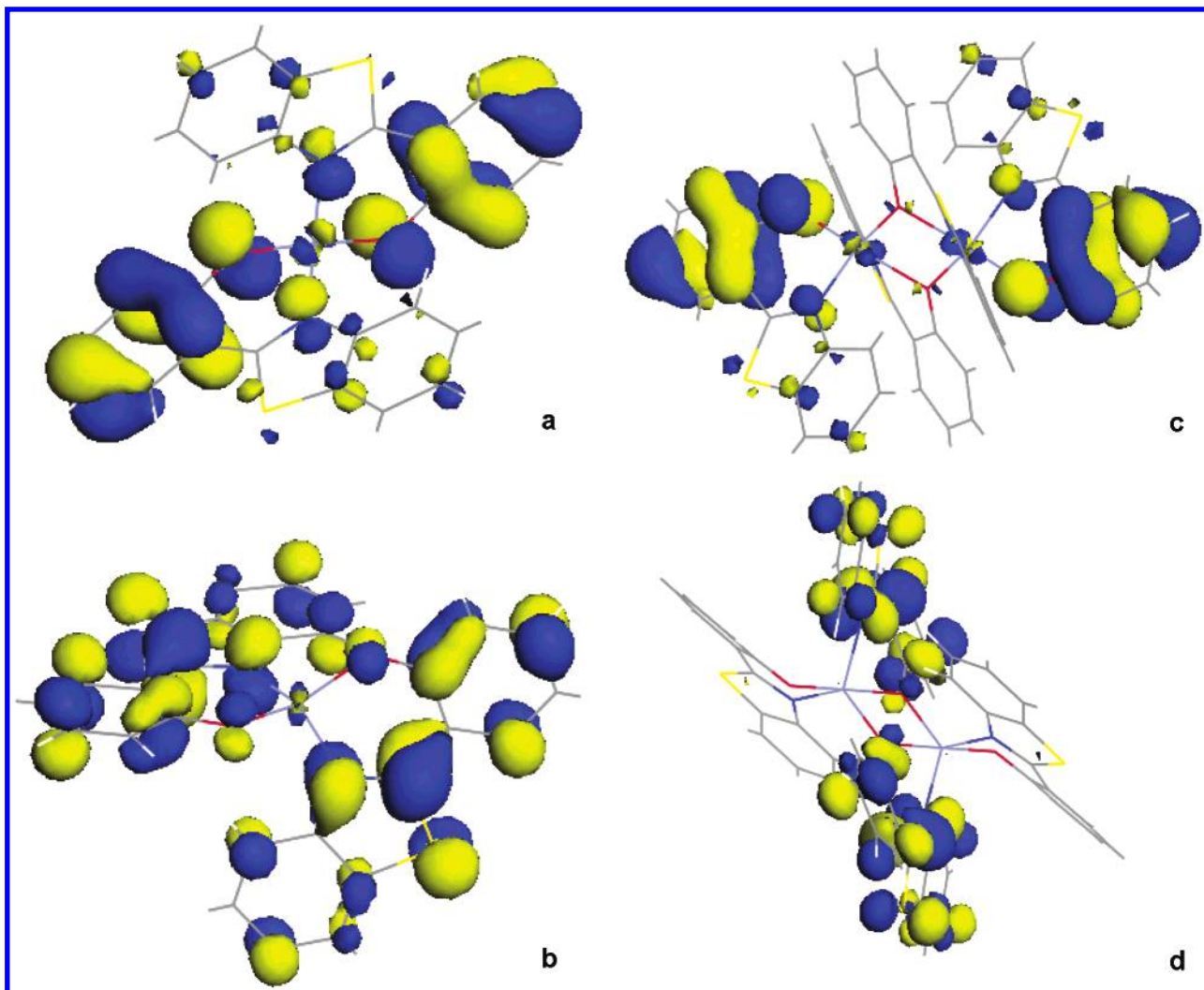
Figure 5. Molecular orbital amplitude plots of the (a) HOMO of the $Zn(BTZ)_2$ molecule, (b) LUMO of the $Zn(BTZ)_2$ molecule, (c) HOMO of the [Zn-$(BTZ)_2]_2$ molecule, and (d) LUMO of the $[Zn(BTZ)_2]_2$ molecule.

Figure 6. Diagram of the calculated orbital energy levels for $Zn(BTZ)_2$ and $[Zn(BTZ)_2]_2$ molecules.

bridging ligands. The main structure distortions in both the cation and the anion relative to the neutral molecule are consistent with this picture. Table 4 lists the variation in the Zn−O and Zn−N distances and the Zn bond angles which are the ones most strongly affected by charge injection. Adding a hole has more pronounced effects than adding an electron. Changes in the distribution of the Zn bond angles are invariably

negligible (at most 1°) and the bond lengths in the rings vary by less than 0.01 Å on average. Change of the Zn bond lengths is mainly localized on the Zn−O bonds of the nonbridging ligands and the Zn−N bonds of the bridging ligands. In the cation, the Zn−O distances of the nonbridging ligands increase and the other Zn bond lengths decrease. A similar effect is found in the anion, except an increase in the Zn−N bond length of the nonbridging ligands and Zn−O bond length of the bridging ligands. Such a structural relaxation behavior is consistent with an increase in the overall positive charge or negative charge in the coordination sphere around zinc. Based on the small structural relaxation for both the cation and the anion discussed above, we should expect that the $[Zn(BTZ)_2]_2$ molecule will exhibit a relatively high structural stability versus the injection of one charge, specifically negative.

In Table 5 we show the calculated values of the IPs and the electron affinities (EAs) for $Zn(BTZ)_2$ and $[Zn(BTZ)_2]_2$. We note that (i) the structural relaxation energies are rather different and (ii) all the values reported here are dependent sensitively on the molecular structures. For the dimer, the energy cost to create an electron is ~1.9 eV and that to extract a hole is ~6 eV, while the experimental value obtained from the UPS is 5.16 eV. However, we note that for the monomer the IP values

Table 4. Calculated Variation of Structural Parameters in the Cation and the Anion for [Zn(BTZ)$_2$]$_2$, Relative to the Neutral Molecules[a]

	cation	anion		cation	anion
Zn(1)−O(1)	0.018	0.009	O(1)−Zn(1)−N(1)	−0.592	−0.459
Zn(1)−O(2A)	−0.002	−0.003	Zn(1A)−O(2)−Zn(1)	0.852	−0.240
Zn(1)−O(2)	−0.010	0.006	O(2A)−Zn(1)−N(1)	0.869	−0.431
Zn(1)−N(1)	−0.005	0.002	O(2)−Zn(1)−N(1)	−0.695	−0.365
Zn(1)−N(2)	−0.019	−0.011	O(1)−Zn(1)−N(2)	−0.694	−0.286
O(1)−Zn(1)−O(2A)	−0.666	0.582	O(2A)−Zn(1)−N(2)	0.752	0.494
O(1)−Zn(1)−O(2)	−0.324	−0.111	O(2)−Zn(1)−N(2)	0.657	0.986
O(2A)−Zn(1)−O(2)	0.342	0.012	N(1)−Zn(1)−N(2)	−0.342	−0.022

[a] Bond lengths are reported in angstroms and bond angles in degrees.
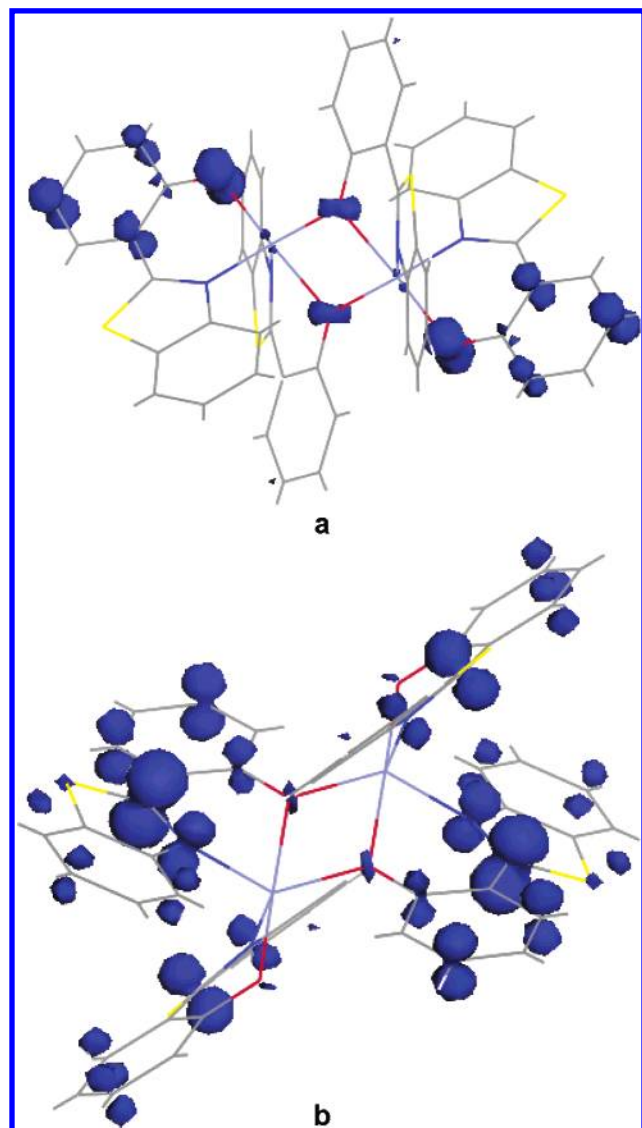
***Figure 7.*** Spin density surfaces of the cation (a) and the anion (b) for the [Zn(BTZ)$_2$]$_2$ molecule.

Table 5. Calculated Ionization Potentials and Electron Affinities for the [Zn(BTZ)$_2$]$_n$ Series (in eV)[a]

| [Zn(BTZ)$_2$]$_n$	IP(v)	IP(a)	EA(v)	EA(a)
Zn(BTZ)$_2$, monomer	6.79	6.74	1.59	1.64
[Zn(BTZ)$_2$]$_2$, dimer	6.18	6.13	1.83	1.89

[a] (v) and (a) indicate vertical and adiabatic values.

increase to ∼6.8 eV, whereas the EA values decrease to ∼1.6 eV.

Electroluminescent Properties. Direct comparison of the EL properties between bilayer devices based on the bilayers NPB/
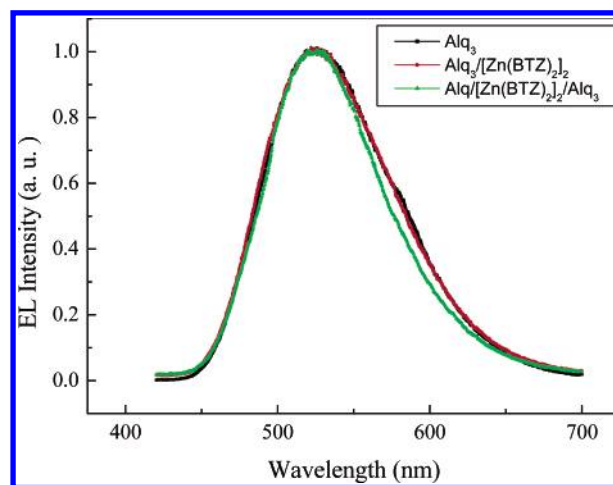
Figure 8. EL spectra of the three devices with different electron transport layers including Alq$_3$ only, Alq$_3$/[Zn(BTZ)$_2$]$_2$, and Alq$_3$/[Zn(BTZ)$_2$]$_2$/Alq$_3$.
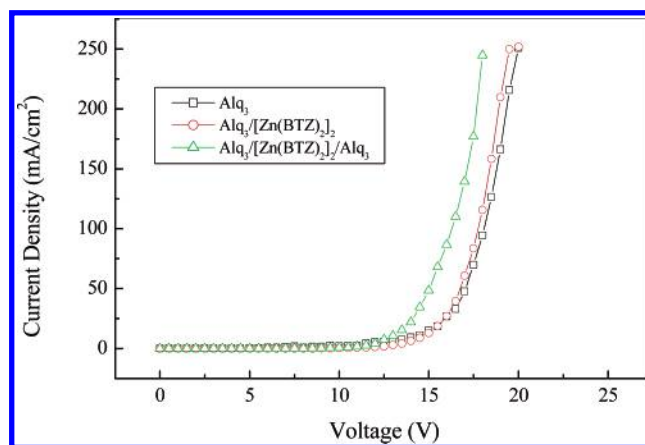
Figure 9. *I−V* characteristics of the three devices with different electron transport layers including Alq$_3$ only, Alq$_3$/[Zn(BTZ)$_2$]$_2$, and Alq$_3$/[Zn(BTZ)$_2$]$_2$/Alq$_3$.

Zn(BTZ)$_2$ and NPB/Alq$_3$ is not adequate due to their different emission characteristics. However, it is appropriate to compare the electron transport properties of [Zn(BTZ)$_2$]$_2$ with that of Alq$_3$ using the following device structures: ITO/NPB(60 nm)/ Alq$_3$(60 nm)/Al (device A), ITO/ NPB(60 nm)/Alq$_3$(30 nm)/ [Zn(BTZ)$_2$]$_2$(30 nm)/Al (device B), and ITO/NPB(60 nm)/ Alq$_3$(30 nm)/[Zn(BTZ)$_2$]$_2$(20 nm)/Alq$_3$(10 nm)/Al (device C). The three devices have the same EL spectra, which are similar to the PL spectrum of Alq$_3$ (see Figure 8). This result indicates that the origin of a blue-green emission with CIE coordinates of $x = 0.353$ and $y = 0.544$ is attributed to the intrinsic emission of Alq$_3$. Figure 9 shows the I−V characteristics of the three devices with different electron transport layer, including Alq$_3$-only, Alq$_3$/[Zn(BTZ)$_2$]$_2$, and Alq$_3$/[Zn(BTZ)$_2$]$_2$/Alq$_3$. The cor-
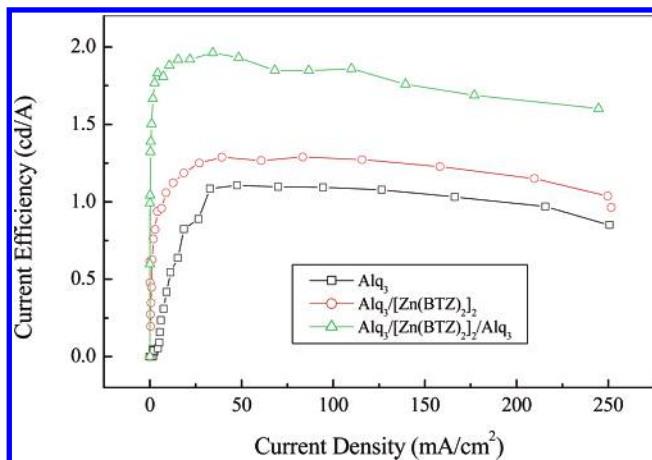
Figure 10. Current density−quantum efficiencies characteristics of the three devices with different electron transport layers including Alq_3 only, Alq_3/$[Zn(BTZ)_2]_2$, and Alq_3/$[Zn(BTZ)_2]_2$/Alq_3.
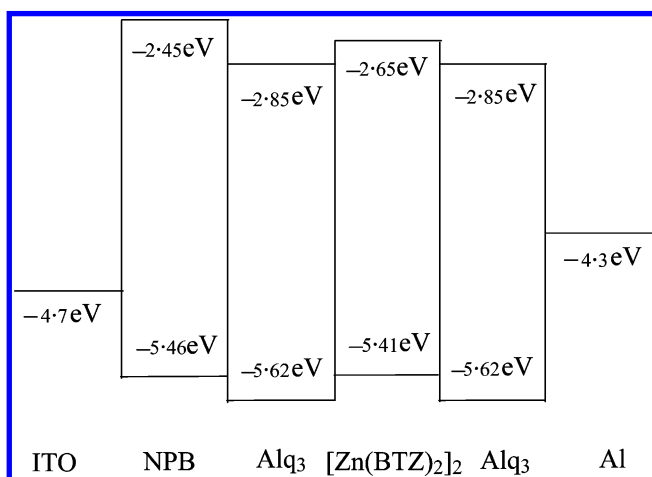
Figure 11. Energetic position of the HOMO and LUMO of the different organic layers (NPB, $[Zn(BTZ)_2]_2$, and Alq_3) and the work function of ITO and Al.

responding quantum efficiencies (QEs) are shown in Figure 10. It is clear that device B with Alq_3/$[Zn(BTZ)_2]_2$ layers has similar turn-on voltage and slightly increased quantum efficiencies compared device A with the Alq_3-only layer, however, the performance of device C with Alq_3/$[Zn(BTZ)_2]_2$/Alq_3 layers is greatly improved over that of the device with Alq_3 only. In fact, the maximum QE of device C with Alq_3/$[Zn(BTZ)_2]_2$/Alq_3 layers is about 1.8 times higher (1.96 cd/A versus 1.1 cd/A) than those obtained from the device A with the Alq_3-only layer, which indicates that a better hole/electron balance is attained within the emissive layer. It is well-known that balanced injection and transport of electrons and holes are crucial in achieving high quantum efficiency. The facility of charge injection depends on the barriers between the molecular frontier orbitals of the organic material and the work function of the contact electrodes. The enhancement of QE for devices B and C compared with that of device A having the same hole injection electrode (ITO) is probably ascribed to a different electron injection barrier at the Alq_3/Al and $[Zn(BTZ)_2]_2$/Al interfaces or different electron transport properties for Alq_3 and $[Zn(BTZ)_2]_2$ layers. Figure 11 shows the energetic position of the HOMO and LUMO of the different organic layers (NPB, $[Zn(BTZ)_2]_2$ and Alq_3) and the work function of ITO and Al. As stated above, the LUMO energy of $[Zn(BTZ)_2]_2$ is −2.65 eV,

determined from the HOMO energy obtained from UPS data and the optical band gap estimated from the absorption onset. Comparing the energy level to that of Alq_3 (LUMO ∼ −2.85 eV), it is clear that the Zn complex has the higher electron injection barrier with regard to the Alq_3. We expect, however, a difficult electron injection from the Al electrode into $[Zn(BTZ)_2]_2$ will reduce the current density and emission efficiency of the devices. In fact, we consider that the largest contribution to the efficiency increase comes from the better electron transport property of $[Zn(BTZ)_2]_2$. In addition, the increase of electron concentration in the emissive layer is responsible for a better charge carrier balance and therefore for the higher efficiency. By introducing the Zn complex within the Alq_3 layer as an electron transport layer, the effects of the electron injection barriers on the EL properties can be removed. Therefore, the better EL characteristics for device C with Alq_3/$[Zn(BTZ)_2]_2$/Alq_3 layers are the consequence of an excellent electron transport of the zinc complex. Furthermore, these findings indicate that $Zn(BTZ)_2$ exhibits a better electron transport property as compared with Alq_3.

The effects of different cathode designs on the turn-on voltage and emission efficiency was examined for the devices with different-electron transport layers including Alq_3 and Alq_3/$[Zn(BTZ)_2]_2$/Alq_3. It was found that LiF/Al would be a better cathode than Al. In the device ITO/NPB(60 nm)/Alq_3(60 nm)/ LiF/Al, inclusion the $[Zn(BTZ)_2]_2$ layer within the Alq_3 layer as an electron-transport layer leads to a clear increase of emission efficiency (from 1.96 to 3.21 cd/A). Simultaneously, use of the LiF/Al cathode for the device with Alq_3/$[Zn(BTZ)_2]_2$/ Alq_3 layers decreases the turn-on voltage (from 12 to 5 V). In general, devices with Alq_3/LiF/Al as the cathode offered higher efficiencies and lower turn-on voltages. In fact, it can be said that the combination of Alq_3/LiF/Al forms a good electron injector for the LEDs. The device lifetime and degradation are being investigated. No crystallization of the Zn complex during the device operation has been found so far.

Conclusion

We report experimental and theoretical studies of the molecular and electronic structures of 2-(2-hydroxyphenyl)benzothiazolate zinc and its EL properties. The molecular structure of an anhydrous $[Zn(BTZ)_2]_2$ obtained by sublimation was determined by X-ray single-crystal diffraction. The molecule is a dimer and it contains two $[Zn(BTZ)_2]$ units connected by oxygen atoms of 2-(2-hydroxyphenyl)benzothiazolate ligands. Two zinc atoms take identical five-coordinate geometries. The molecular packing involves the close intermolecular $\pi-\pi$ interaction of ligands on adjacent molecules via a benzothiazolyl/ phenolato ring overlap. Thermal analysis and spectroscopic methods show the sole existence of the dimeric structure in powder and thin film. This result is further supported by theoretical calculations of the total energies of $Zn(BTZ)_2$ and $[Zn(BTZ)_2]_2$.

The electronic structures of the $Zn(BTZ)_2$ oligomers are investigated by using quantum chemical calculations. The special nature of the HOMO's and LUMO's is clarified in detail. The HOMO's of the $[Zn(BTZ)_2]_2$ molecule are mainly localized on two nonbridging ligands, whereas the LUMO's are localized predominantly on two bridging ligands. It is shown that both

the cation and the anion reveal small structural changes relative to the neutral $[Zn(BTZ)_2]_2$ molecule. This zinc complex appears to have a better electron-transport property than that of the well-established electron transporter Alq_3.

Supporting Information Available: X-ray crystallographic data. This material is available free of charge via the Internet at http://pubs.acs.org.

JA0371505